Available online at www.sciencedirect.com
ScienceDirect
Journal of Computational Physics 221 (2007) 558–576
JOURNAL OF COMPUTATIONAL PHYSICS
www.elsevier.com/locate/jcp

The spatial resolution properties of composite compact finite differencing

Stephen A. Jordan *

Naval Undersea Warfare Center, Code 74, Bldg. 1346/4, 1176 Howell Street, Newport, RI 02841, United States

Received 12 January 2006; received in revised form 16 June 2006; accepted 20 June 2006
Available online 1 August 2006

Abstract

Demand for spectral-like spatial routines to resolve fine-scale physics is easily satisfied by compact finite differencing. Commonly, the lower-order multi-parameter families at (and near) non-periodic boundaries are independently tuned to meet or exceed the high-order resolution character of the field stencil. Unfortunately, that approach quantifies a false influence of the boundary scheme on the resultant interior dispersive and dissipative consequences of the compound template. Knowing that each composite template owns three ingredients that define their numerical character, only their formal accuracy and global stability have been properly treated in a coupled fashion. The present work presents a companion means for quantifying the resultant spatial resolution properties. The procedure particularly focuses on the multi-parameter families used to diminish the dispersive and dissipative errors at the non-periodic boundaries. The process introduces a least-squares technique of the target field stencil to optimize the free parameters of the boundary scheme. Application of the optimized templates to both the linear convection and Burgers equations at a fictitious non-periodic boundary showed major reductions of the predictive error.

Keywords: Compact finite differencing; Numerical methods; Resolution errors; Dispersive errors; Dissipative errors

1. Introduction

Not surprisingly compact finite differences for approximating derivatives is a popular choice when resolving fine-scale physics. The spatial resolution and order increase dramatically over comparable standard explicit schemes when differencing the same number of grid points. Highest orders can reach spectral-like spatial resolution while simultaneously treating a wide range of boundary conditions. This fact is especially beneficial for efficiently resolving the smaller spatial scales near the boundaries in complex applications. Often nearly three-fourths of the resolvable scales in the field hold a resolving efficiency of 90% or better. Both conservative and non-conservative forms of the governing formulations are easily handled by compact differencing. One notable sacrifice of improving the spatial resolution and order is the potential loss of smooth solutions as well as

* Tel.: +1 401 832 1383.
E-mail address: jordansa@npt.nuwc.navy.mil.

0021-9991/$ - see front matter
doi:10.1016/j.jcp.2006.06.026

temporal stability. But these drawbacks have been thoroughly investigated since inception of compact differencing with remedial measures now clearly understood.

Early applications of compact finite differencing include Hirsh [1] who centered on resolving the steady fluid physics of a Blasius boundary layer and shear driven cavity using the standard fourth-order Pade-type scheme. While the former application approximated the boundary derivatives by a one-sided time-lagged explicit formulation, the latter solutions evaluated the boundary derivative using a Pade-type approximant. Given the same number of grids points necessary for standard second-order differencing, Hirsh demonstrated fourth-order solution accuracy of the Pade-type scheme. Soon afterward, Adam [2] introduced third-order one-sided compact differencing to circumvent exterior fictitious points as required to uphold the interior scheme at the boundary. An early treatment of formal error in compact finite differencing came from Gustafsson [3] who realized pth interior accuracy of a hyperbolic system with at least a $p\text{th} - 1$ definition prescribed at the boundary. Christie [4] found unacceptable numerical oscillations of the fourth-order Pade-type stencil for applications dominated by convection, but alleviated this behavior by simply introducing an upwinding component. Other early applications of Pade-type stencils dealt with resolving the fine-scale turbulent physics through advanced methodologies such as direct numerical and large-eddy simulations (DNS and LES). As an example, Mansour et al. [5] compared the fourth-order Pade-type scheme in their LES computations against the same order (lower resolution) explicit central method for resolving the decay of isotropic turbulence (periodic boundary conditions). Inasmuch as the filtering technique and subgrid-scale model shadowed the salient effects of the different discretization choices, Mansour et al. found no discernible improvements in the turbulent energy spectra by switching to the compact scheme. Later, Sandham and Reynolds [6] mixed a spectral technique with a modified sixth-order Pade-type scheme [7] to reach DNS resolution in the non-reflecting non-periodic direction of a compressible mixing layer. They also successfully tested their mixed numerics for resolving the small-scale secondary instabilities of a similar but incompressible layer at low Mach number ($Ma = 0.4$).

With the continuous rising demand for realistic applications whose solutions call for high resolution as well as complex topologies and boundary conditions, compact finite differencing is aptly replaced costly spectral developments. For instance, Joslin [8] introduced a conservative sixth-order Pade-type template with fourth-order compact stencils at the boundary and first field points to resolve the fine scale instabilities along the attachment-line direction in a swept Hiemenz flow. This choice coupled with a Chebyshev series gave results that illustrated the Hiemenz flow as an acceptable model of the transition mechanism along swept wings. One of the first uses of compact upwinding comes from Adams and Shariff [9] for shock capturing. Their high-order upwind stencil supplied enough numerical dissipation to be combined with an essentially non-oscillatory (ENO) procedure for dampening the under-resolved smallest scales of the shock-turbulence communication.

Besides fluid physics, compact finite differencing has recently emerged with great success in computational acoustics. Compact schemes are preferred over standard explicit differencing in this discipline because they can potentially lower the dispersive (and dissipative) errors in the numerical approximations of the short waves. For example, Hixon and Turkel [10] developed a high-order compact MacCormack-type scheme for computational aeroacoustics (CAA) that retained fourth-order accuracy in both the forward and backward operators. They exercised their stencil against three sample problems as chosen from the first and second CAA workshops [11,12]. Likewise, Kim and Lee [13] extracted problems from the first CAA workshop to test their highly optimized template that housed several compact stencils including one-sided schemes at the boundaries and the adjacent first and second interior points. More recently, Popescu et al. [14] found improve preservation of the nonlinear wave profile when the finite difference versions of the Dispersion-Relation-Preserving [15] and optimized-prefactored-compact [16] schemes were reformulated into a finite volume molecule. Given the many successes such as these mentioned above, applications of compact finite differencing over the past decade has grown immensely spanning both internal and external topologies that involve complex physics such as combustion [17], cavitation [18], and electrodynamics [19]; as well as many other provocative phenomena.

One can easily assess the spatial resolution and temporal stability properties of their particular compact differencing strategy by employing Fourier analysis. The real components of the resultant modified wavenumbers measure the dispersive nature of the stencil while the imaginary elements indicate expected dissipation. Apart from any boundary influence, only the odd ordered stencils will dampen the high wavenumber spectral

energy. Undoubtedly, Lele [7] presented the most comprehensive Fourier treatment of compact finite differencing that included one-sided stencils to close the field solutions given non-periodic boundary conditions. He illustrated spectral-like resolution of the larger stencils by fine-tuning the free parameters that can arise through reduction in the formal order. He also demonstrated global stability of several Pade-type templates (including non-conservative boundary effects) by conducting a modal analysis of the discretized linear convection equation. Similarly, Carpenter et al. [20] examined global pth accuracy and GKS stability [16] of both the fourth- and sixth-order Pade-type stencils as coupled with a broad mixture of compact definitions at the boundary and first field points (sixth-order only). Those mixtures of the multi-parameter family that were found conditionally unstable, but globally accurate, were tuned until all eigenvalues of the final template fell inside the left-half plane of the stability spectrum.

When designing a compact finite differencing strategy for approximating the governing formulation of a physical event, one must be careful about preserving the intended accuracy, stability and resolution. With cyclic end-conditions these attributes are formally equivalent both locally and globally. But non-periodic boundaries can potentially erode their projected gains. Their own spatial resolution properties can propagate well into the adjacent field. As discussed above, certain one-sided stencils selected for the latter boundary derivatives (as well as those near boundary points for very high field accuracy) degrade both the accuracy and stability of the field template. The inclusive works of Lele [7] and Carpenter et al. [20] proved that the respective analyses must treat the composite template to quantify the resultant spatial accuracy and temporal stability from a global perspective. Unfortunately, no such companion treatment presently exists for understanding the operative field resolution.

In the present paper, we will investigate the influence of various compact boundary stencils on the adjacent field spatial resolution. Spatial resolution differs from spatial accuracy in a sense that two separate stencils can own the same truncation error, but resolve the physical wave quite differently. We will deviate from the present standard practice of quantifying the spatial resolution character of each stencil separately and locally. The procedure actually takes a path similar to Lele's Fourier exercise on universal stability, except herein we quantify the linked dispersive and dissipative errors of the composite template. We will place strong emphasis on the family of multi-parameter stencils where the free-parameters are finely tuned to match the field scheme. In most cases, the boundary (and near boundary) stencils couple poorly with the field template even though their appearance is attractive locally. Corrective measures include an optimizing strategy for the free parameters of the lower-order boundary schemes to achieve a preferable spatial resolution in the field. Finally, this proposed procedure completes the recommended tri-testing (accuracy, stability and resolution) of a particular composite compact template to understand the prevailing numerical properties through the entire solution domain before beginning the computation.

2. Compact finite differencing

As emphasized earlier, compact finite differencing is widely accepted as a viable direction towards improved spatial resolution and/or higher accuracy over traditional explicit schemes. Their derivation is accomplished by appropriately satisfying the summation of respective coefficients in the Taylor series expansions of each constituent. Both the neighboring quantities as well as their exact derivatives are treated in the series approximation. Theoretically, the compact variety increases the spatial accuracy by two orders over their companion explicit scheme. Inasmuch as the compact stencils are implicit, they require inversion of the multi-diagonal coefficient matrix that raises the overall CPU requirement. Frequently, this added CPU cost is negligible relative to the overall computational expense of practical applications.

2.1. Spatial resolution

When attempting to properly resolve the smallest spatial scales, the advantages of high-order compact finite differencing become quite clear. This fact is easily quantified by differentiating the basic Fourier wave $q(x) = e^{ikx}$ and profiling its compact differencing approximation over the range of resolvable wavenumbers (up to the π wave). First, we will adopt the same nomenclature as Lele [7] where k and x are defined as the dimensionless complex wavenumber and coordinate of the wave $q(x)$. The dependent variable k resides inside

the periodic domain [0, π]. Exact differentiation of $q(x)$ with respect to x simply yields $q'(x)_{\mathrm{ex}} = \mathrm{i}kq(x)$ where full resolution of k ascribes a spectral method (except $k \neq \pi$). Conversely, compact finite differences approximate the wave derivative as $q'(x)_{\mathrm{fd}} = \mathrm{i}\hat{k}q(x)$ where $\hat{k}$ is defined as the dimensionless complex modified wavenumber. Deviations of the real and imaginary elements of $\hat{k}$ from those of k are the key ingredients for measuring the stencil resolution character. Notably, each stencil owns a unique distribution of $\hat{k}$ within the periodic domain.

A simple example for illustration purposes is the popular fourth-order Pade-type approximation of the first-order derivative centered over the ith point;

$$q'_{i+1} + 4q'_i + q'_{i-1} = 3(q_{i+1} - q_{i-1})/\Delta \tag{2.1}$$

where Δ denotes the dimensionless local discrete point spacing. The variable q on the right side of (2.1) must be known at neighboring points $i \pm 1$. Substituting the exact Fourier wave expression for the q variable and its derivatives at these discrete points gives a complex form of the modified resolvable wavenumber ($\hat{k} = \hat{k}_{\mathrm{r}} + \mathrm{i}\hat{k}_i$). For the fourth-order Pade-type expression, $\hat{k}$ is only real valued ($\hat{k}_i\Delta = 0.0$) and defined as

$$\hat{k}_{\mathrm{r}}\Delta = \frac{3/2\sin(k\Delta)}{1 + 1/2\cos(k\Delta)} \tag{2.2}$$

Lele [7] introduced the numerical limit of resolving efficiency [$e(\delta)$] that quantifies the fraction of *well-resolved* waves by a particular differencing stencil; $e(\delta) = (k\Delta)_\delta/\pi$ Herein, we define the quantity δ as the resolution expectancy that is specified by the user; $\delta_{\mathrm{r,i}} = 1 - |1 - (\hat{k}\Delta)_{\mathrm{r,i}}/(k\Delta)_\delta|$. Given this measure, 59% [$e(\delta_{90}) \leqslant 0.59$] of the resolvable waves are efficiently resolved 90% ($\delta_r \geqslant 0.90$) or better by the fourth-order Pade-type scheme (see Table 1). Under the same computational molecule, this efficiency is well over 200% better than the standard explicit second-order stencil [$e(\delta_{90}) \leqslant 0.25$]. Thus, compact differencing is much more spectral-like than its explicit analog and leads to superior resolution of the finer resolvable scales. This dramatic improvement easily explains the recent gravitation toward compact finite differencing. Demand for a more strict tolerance such as 95% (notation δ_{95}) reduces the resolving efficiency of the fourth-order Pade-type scheme to just over 50% [$e(\delta_{95}) \leqslant 0.50$], which may call upon finer gridding to sufficiently resolve the fine-scale physics.

2.2. Interior schemes

Interior schemes difference the neighboring quantities and their derivatives either symmetrically (central) or asymmetrically (upwind) about the point of interest. They can be successfully applied throughout domains having periodic boundary conditions as well as the interior nodes that are sufficiently away from non-periodic boundaries to complete the explicit side of the stencil. The upwind category is most suitable for high-order approximations of the non-conservative nonlinear terms in the governing equations. The compact stencils studied in the present paper have the form

$$aq'_{i+1} + bq'_i + cq'_{i-1} = \eta q_{i+2} + \lambda q_{i+1} + \alpha q_i + \gamma q_{i-1} + \beta q_{i-2} \tag{2.3}$$

where the variable q is known at the center (i) and neighboring points $i \pm 1$ and $i \pm 2$ throughout the domain to reach fourth-, fifth- and sixth-order accuracy. Their respective coefficients η, λ, α, γ, β are listed in Table 1 along with the set a, b and c of the variable derivative q' at points i and $i \pm 1$. Listed in the table is the resolving efficiency of each compact stencil given an expected resolution efficiency of 90%. Interestingly, the fifth-order

Table 1
List of coefficients and spatial resolution for several interior compact finite differencing stencils; 4–6: formal order

Order	Coefficients: compact finite differences								Resolution
	a	b	c	η	λ	α	γ	β	
4c	1.0	4.0	1.0	–	3.0	–	3.0	–	0.59
5c	3.0	18.0	9.0	–	10.0	9.0	−18.0	−1.0	0.78
6c	12.0	36.0	12.0	−1.0	28.0	–	−28.0	1.0	0.70

upwind scheme (5c) provides at least 90% efficiency over 78% of the resolvable waves, which is a 10% improvement over the higher-order central stencil (6c) [$e(\delta_{95}) \leqslant 0.70$]. But this enhancement is often masked by the inherent high dissipative error associated with upwind finite differencing over nearly one-half of the resolvable wavenumbers.

Distribution of the modified wavenumber in the exact wavenumber space quantifies the dispersive and dissipative errors of the finite-difference scheme. Exclusive of any time differencing errors, deviation of the real part from the exact wavenumber measures the degree of dispersion (or phase error) while the imaginary half indicates the level of expected dissipation. Both of these behaviors are obviously undesirable when attempting to resolve the finest spatial scales, but they can be diminished through fine gridding techniques and/or high-resolution differencing templates. These conventional options are easily illustrated by approximating the one-dimensional propagation of a linear wave as defined by

$$u_t + cu_x = 0 \tag{2.4}$$

with the wave speed $c = 1$ for brevity. Given the initial condition

$$u(x, t = 0) = \frac{1}{2} e^{-\ln 2(x/n)^2} \tag{2.5a}$$

the exact solution for all time becomes

$$u(x, t) = \frac{1}{2} e^{-\ln 2(x'/n)^2} \tag{2.5b}$$

where $x' = x - x_0 - t$. The spatial resolution of the simulation is defined by ratio $\Delta x/n$ where Δx is the uniform one-dimensional grid spacing. To avoid adverse time differencing and stability errors, the linear wave was time-advanced herein by the Euler method (first-order) with the stability coefficient set to a very small value (CFL $\ll 1.0$).

Fig. 1 shows the spatial distribution of the real (dispersive error) and imaginary (dissipative error) elements of the modified wavenumber for the present compact stencils. One can clearly see that the upwind stencil (5c) will reduce the dispersive error at a preferred cost of induced dissipation for nearly half of the resolvable wavenumbers. The lack of inherent dissipation in the central 4c and 6c schemes (fourth-order and sixth-order, respectively) is readily evident in Fig. 2 ($t = 400$) as suggested by their oscillatory resolution of the linear wave. At a relatively coarse grid spacing $k\Delta \sim 2.3$, the resolution efficiency of the central 4c scheme is only 63% ($\delta_r = 0.63$) and attributes to the highest phase error. Conversely, the same uniform spacing ($k\Delta \sim 2.3$) when implementing the upwind-biased stencil dramatically improves the resolution efficiency to 95%, which is suf-

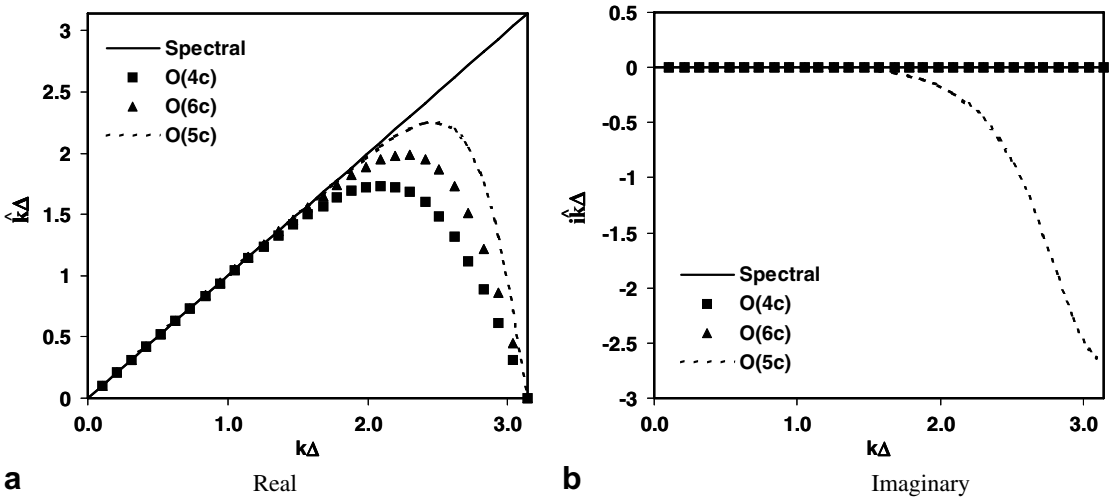

Fig. 1. Real (dispersive error) and imaginary (dissipative error) distributions of modified wavenumbers ($\hat{k}\Delta$) for fourth-order (4c), fifth-order (5c) and sixth-order (6c) compact finite differences.

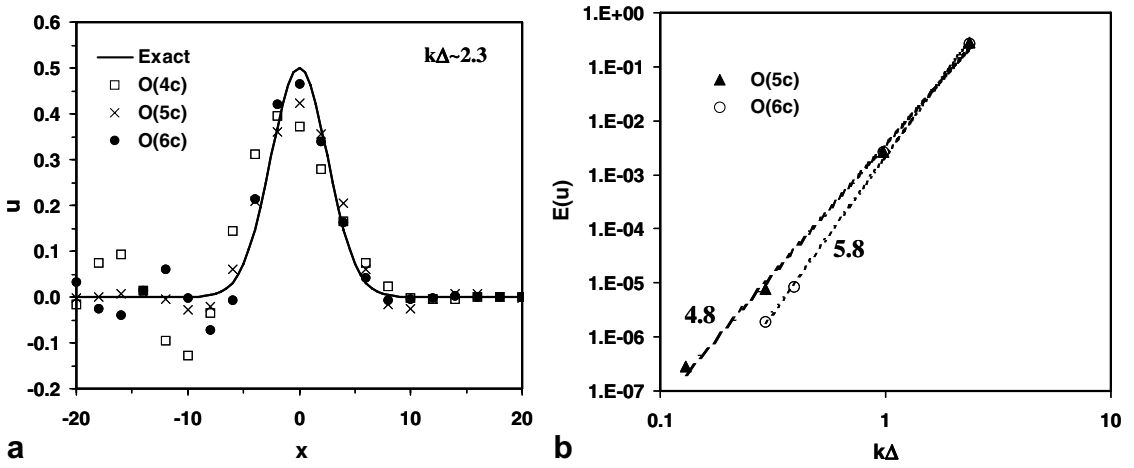

Fig. 2. Solutions (a) and predictive error (b) of the linear wave equation using 4c, 5c and 6c finite difference schemes for the first-order term at various grid spacing ($k\Delta$).

ficient to control the phase error while dampening the oscillations. This result confirms why upwind differencing is often chosen to control the phase and aliasing errors in regions of moderate gridding. But the induced dissipation ($\delta_i = -0.47$) of the 5c stencil, although owning lowest dispersive error, broadens the wave base while under-predicting the wave peak. Convergence of the 5c and 6c stencils with reduced grid spacing is plotted in Fig. 2b; $E(u) = \sum(u_e - u_{fd})$ where u_e and u_{fd} are the exact and predicted waves at time $t = 400$. This log-log plot verifies formal accuracy of the 5c and 6c stencils by calculating the slope of $E(u)$ under finer grid spacing ($k\Delta$).

2.3. Non-periodic boundary schemes

The compact variety of non-periodic boundary schemes is typically one-sided (no fictitious points) and should be no lower than one-order from the field scheme to preserve the respective formal spatial accuracy. Their harmful effects on global numerical stability and accuracy have been thoroughly investigated by others using various techniques [3,7,10,20]. Theoretically, the spatial order of a compact boundary stencil is unlimited (given enough interior points), but their coupled resolution properties are actually far different from the adjacent field scheme. This fact is especially notable for the multi-parameter families. Herein, we will couple both standard (no free parameters) and two-parameter one-sided compact schemes up to fourth-order accuracy with the above interior schemes. The general expression of the former stencil has the form,

$$aq'_2 + bq'_1 = \lambda q_4 + \alpha q_3 + \gamma q_2 + \beta q_1 \tag{2.6}$$

where the first point lies on the boundary. Table 2 lists values for all the coefficients in (2.6) which reflect forward projection of the stencil onto the adjacent interior nodes. Although tempting to examining the local dispersive and dissipative errors of this boundary stencil, it is actual quite futile at this point because these characteristics are strongly influenced by the adjacent field scheme and vice versa.

Table 2
List of coefficients for several compact one-sided differencing stencils; 2–4: formal order

Order	Coefficients: compact one-sided differences					
	a	b	λ	α	γ	β
2c	2.0	2.0	–	–	1.0	−1.0
3c	4.0	2.0	–	1.0	4.0	−5.0
4c	18.0	6.0	−1.0	9.0	9.0	−17.0

Reducing the dispersive and dissipative errors of the compact boundary stencil in (2.6) is possible by either compromising accuracy or projecting the stencil further into the interior domain. The new coefficients of both stencils become free parameters that are selectively constrained to reach a desired result. Choosing the former approach, Lele [7] constrained the two parameters of the second-order-accurate version of (2.6) to give negligible dissipation over all resolvable wavenumbers. Alternatively, projecting the stencil forward over two additional field points preserves the fourth-order accuracy that simply appears as

$$aq'_2 + bq'_1 = \eta q_6 + \xi q_5 + \lambda q_4 + \alpha q_3 + \gamma q_2 + \beta q_1 \tag{2.7}$$

where (a, η) are considered the free parameters; one each from the explicit and implicit sides of the two-parameter family. The remaining coefficients in terms of these parameters are defined by $(b = 1)$

$$\xi = \frac{-3 + a - 60\eta}{12}, \quad \lambda = \frac{8 - 3a + 60\eta}{6}, \quad \alpha = \frac{-6 + 3a - 20\eta}{2},$$
$$\gamma = \frac{24 - 5a + 30\eta}{6}, \quad \beta = -\frac{25 + 3a + 12\eta}{12} \quad \text{(fourth-order)} \tag{2.8}$$

One should note that this two-parameter boundary stencil becomes fifth-order accurate as a one-parameter family or a sixth-order-accurate scheme when all the coefficients are evaluated through Taylor series expansions of their associate variables. We can also reduce (2.8) to a third-order-accurate two-parameter family $(a, \xi, \eta = 0)$ as defined by

$$\lambda = \frac{2 - a - 24\xi}{6}, \quad \alpha = \frac{-3 + 2a + 12\xi}{2}, \quad \gamma = \frac{6 - a - 8\xi}{2},$$
$$\beta = \frac{-11 - 2a + 6\xi}{6} \quad \text{(third-order)} \tag{2.9}$$

which becomes fourth-order accurate as a one-parameter family or fifth-order accurate with all coefficients defined uniquely. In the next section, we will study the prominent differences between local and projected spatial resolution errors of these multi-parameter stencils when coupled with compact fourth, fifth and sixth-order interior schemes.

3. Composite templates

A composite template is defined herein as one carrying at least two different compact finite difference stencils. One of the stencils in the present templates is a boundary scheme, but this composition is not necessarily a limiting factor. We will study templates owning field schemes whose explicit elements extend beyond the boundary, therefore requiring low-order symmetric or high-order asymmetric stencils at the adjacent boundary points. Because the composite templates are solved implicitly, the local wavenumber spectrum is not unique to only the respective stencil. We emphasize that the individual spectra are locally connected and must be quantified accordingly. This process deviates from previous evaluations that dealt with assessing the dispersive and dissipative nature of composite templates. Previous analyses examined the resolution errors of each stencil separately. But that approach produces a false understanding of the local errors. This deception is notably important when multi-parameter stencils are finely tuned to the field scheme. In particular, the free-parameters of the boundary stencil are adjusted to reproduce a spectrum that closely mimics the adjacent interior scheme. We will observe in the following section, that a decoupled analysis of the resultant composite template will produce misleading profiles of the modified wavenumber spectra because the participating stencils are not treated properly as communicative members.

3.1. Modified wave number

To correctly evaluate the modified wavenumber spectra of a composite template, we must first represent the contributing stencils as a coupled linear system. This system may appear as

$$Aq' = R(q)/\Delta \tag{3.1}$$

where A is a tri-diagonal matrix comprised of the coefficients of the derivative vector (q') and $R(q)$ is a vector of the explicit elements. After substituting the approximated derivative $q'(x)_{\mathrm{fd}}$ of the basic Fourier wave into (3.1), a second linear system is produced that can be represented as

$$\mathrm{i}[G(k\Delta)]\{\hat{k}\Delta\} = H(k\Delta) \tag{3.2}$$

where $G(k\Delta)$ is a $N \times N$ tri-diagonal matrix and $H(k\Delta)$ is a N length vector. The variable N denotes the number of nodal points holding a complete modified wavenumber spectrum over the same resolvable scales ($k\Delta \leqslant \pi$). A good test for applying (3.2) is the composite template of Lele [7] that was implemented by Chung and Luo [21] for resolving the heat transfer of an impinging jet. Their composite template comprised a sixth-order Pade-type interior scheme coupled with a one-sided third-order-accurate expression and fourth-order Pade-type stencil at the boundary and first interior points, respectively. We will use the notation 3-4-6-4-3 to identify this template that denotes the formal order of each stencil extending from boundary to boundary via the field domain. The coefficients of this template are listed in Tables 1 and 2. The matrix $G(k\Delta)$ of the composite template becomes

$$G(k\Delta) = \begin{bmatrix} 2 & 4\mathrm{e}^{\mathrm{i}k\Delta} & & & & & \\ \mathrm{e}^{-\mathrm{i}k\Delta} & 4 & \mathrm{e}^{\mathrm{i}k\Delta} & & & & \\ & 12\mathrm{e}^{-\mathrm{i}k\Delta} & 36 & 12\mathrm{e}^{\mathrm{i}k\Delta} & & & \\ & \vdots & \vdots & \vdots & & & \\ & & 12\mathrm{e}^{-\mathrm{i}k\Delta} & 36 & 12\mathrm{e}^{\mathrm{i}k\Delta} & & \\ & & & \mathrm{e}^{-\mathrm{i}k\Delta} & 4 & \mathrm{e}^{\mathrm{i}k\Delta} & \\ & & & & 4\mathrm{e}^{-\mathrm{i}k\Delta} & 2 & \end{bmatrix} \tag{3.3}$$

with the boundary ($h^{\mathrm{b}+}$), first point (h^{1}) and interior (h^{f}) explicit elements of the vector $H(k\Delta)$ defined by

$$h^{\mathrm{b}+} = -5 + 4\mathrm{e}^{\mathrm{i}k\Delta} + \mathrm{e}^{\mathrm{i}k\Delta} \tag{3.4a}$$

$$h^{1} = 3(\mathrm{e}^{\mathrm{i}k\Delta} - \mathrm{e}^{-\mathrm{i}k\Delta}) \tag{3.4b}$$

$$h^{\mathrm{f}} = 28(\mathrm{e}^{2\mathrm{i}k\Delta} - \mathrm{e}^{-2\mathrm{i}k\Delta}) - (\mathrm{e}^{\mathrm{i}k\Delta} - \mathrm{e}^{-\mathrm{i}k\Delta}) \tag{3.4c}$$

where the subsequent exponent (+) implies one-sided forward differences.

The modified wavenumber spectra of both the coupled and decoupled versions of template 3-4-6-4-3 are plotted in Fig. 3. The coupled profiles represent solutions of the system in (3.2) with definitions ((3.3) and (3.4)) over dimensionless wavenumbers $0 \leqslant k\Delta \leqslant \pi$. Clearly, the disparity between companion profiles is obvious. Two important differences are the false impressions of small dispersive and dissipative errors at the boundary. The dispersive profile of the decoupled stencil (3cb) suggests that 82% [$e(\delta_{90}) \leqslant 0.82$] of the resolvable waves hold at least a 90% resolving efficiency, but this resolution is actually only 28% [$e(\delta_{90}) \leqslant 0.28$] when properly solved as a coupled composite template. At the boundary the actual dissipative error is more than twice that of the decoupled profile over the same upper half of resolvable scales. This higher error propagates well into the adjacent field. As illustrated in Fig. 3b, negligible levels are not detected until after the third interior point. Thus, a significant element of numerical dissipation exists near the boundary of the 3-4-6-4-3 composite template that would be otherwise unknown through separate error analyses of each participating constituent scheme.

3.2. Modified wave number: multi-parameter templates

Probably one of the most deceptive notions of reduced dispersive and dissipative errors at the boundaries comes from fine-tuning the associated free parameters of a multi-parameter stencil to best meet the spatial resolution properties of the field scheme. Mathematically, we simply choose constraints that tend toward the boundary condition $\hat{k}^{\mathrm{b}}_{\mathrm{r,i}} = \hat{k}^{\mathrm{f}}_{\mathrm{r,i}}$ for all resolvable wavenumbers ($k\Delta \leqslant \pi$). Constraints on only the imaginary component can be uniquely fulfilled when compact central differences are chosen to approximate the interior derivatives, but the corresponding real part can only be matched at discrete resolvable wavenumbers ($k\Delta$). For

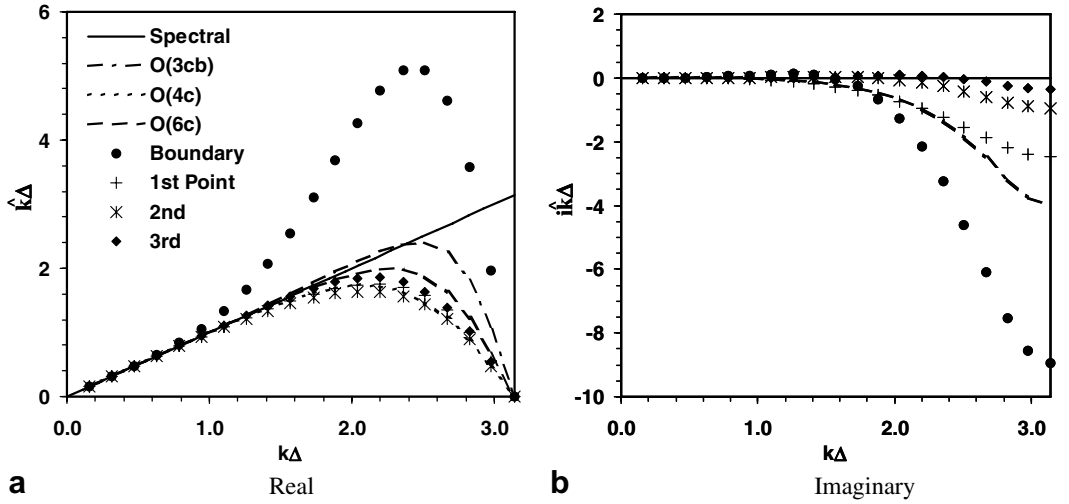

Fig. 3. Real (dispersive error) and imaginary (dissipative error) distributions of modified wavenumbers for composite template 3-4-6-4-3; 3cb, 4c and 6c are the decoupled profiles of the third-, fourth- and sixth-order compact finite difference stencils at the boundary, first and field points, respectively.

instance, only a single parameter would be open for adjustment in the two-parameter boundary stencils to match the entire dispersive error profile of the field scheme. Lele [7] introduced this treatment using a one-sided two-parameter family stencil that was second-order accurate. Adopting the notation in (2.7), the complex form of his stencil ($\eta = \xi = 0$) for the modified wavenumber becomes ($b = 1$)

$$\mathrm{i}(\hat{k}\Delta)^b(b + a\mathrm{e}^{\mathrm{i}k\Delta}) = \lambda\mathrm{e}^{3\mathrm{i}k\Delta} + \alpha\mathrm{e}^{24\mathrm{i}k\Delta} + \gamma\mathrm{e}^{\mathrm{i}k\Delta} + \beta \tag{3.5a}$$

where

$$\alpha = \frac{-1 + a - 6\lambda}{2}, \quad \gamma = 2 + 3\lambda, \quad \beta = \frac{-3 - a - 2\lambda}{2} \quad \text{(second-order)} \tag{3.5b}$$

Given the substitution $\hat{k}^{\mathrm{b}}_{\mathrm{r,i}} = \hat{k}^{\mathrm{f}}_{\mathrm{r,i}}$ where the real component is defined as $\hat{k}^{\mathrm{f}}_{\mathrm{r}} = \mathrm{real}[(\hat{k}\Delta)^{\mathrm{f}}]$, two expressions arise from (3.5a) that reveal the real and imaginary ($\hat{k}^{\mathrm{f}}_{\mathrm{i}}$) components of the interior modified wavenumber in terms of the boundary free parameters (a, λ). These expressions are (not reduced to simplest form)

$$\begin{aligned}&(1 - \cos 2k\Delta - 2\hat{k}^{\mathrm{f}}_{\mathrm{r}}\sin k\Delta - 2\hat{k}^{\mathrm{f}}_{\mathrm{i}}\cos k\Delta)a \\ &\quad = (2\cos 3k\Delta - 6\cos 2k\Delta + 6\cos k\Delta - 2)\lambda + 2\hat{k}^{\mathrm{f}}_{\mathrm{i}} - \cos 2k\Delta + 4\cos k\Delta - 3\end{aligned} \tag{3.6a}$$

and

$$(2\hat{k}^{\mathrm{f}}_{\mathrm{r}}\cos k\Delta - 2\hat{k}^{\mathrm{f}}_{\mathrm{i}}\sin k\Delta - \sin 2k\Delta)a = (2\sin 3k\Delta - 6\sin 2k\Delta + 6\sin k\Delta)\lambda - 2\hat{k}^{\mathrm{f}}_{\mathrm{r}} - \sin 2k\Delta + 4\sin k\Delta \tag{3.6b}$$

Under the field constraint $\hat{k}^{\mathrm{f}}_{\mathrm{i}}(k\Delta = \pi) = 0$, the free parameter ($\lambda$) on the explicit side of the stencil is uniquely defined; $\lambda = -1/2$. After setting the second free parameter to $a = 4$, the adjusted second-order boundary stencil is tuned to the fourth-order Pade-type scheme (notation 2^2-4-2^2). In terms of expected resolution improvement, the new boundary stencil holds a dispersive error $e(\delta_{90}) \leqslant 0.54$ that mimics the interior scheme $e(\delta_{90}) \leqslant 0.59$ as illustrated in Fig. 4a. Likewise, the dissipative error of this stencil (not shown) is nearly negligible for all resolvable wavenumbers. But when the composite template is re-quantified as a strictly linked system, this favorable image changes dramatically (Fig. 4b). The template actually holds only a moderate dispersive error ($\delta_r \leqslant 0.7$) at the boundary over the lower 1/3 of the spectrum $e(\delta_{70}) \leqslant 0.30$. Beyond resolvable wavenumbers $k\Delta \geqslant \pi/2$, this error quickly degrades to several orders of magnitude higher than the decoupled

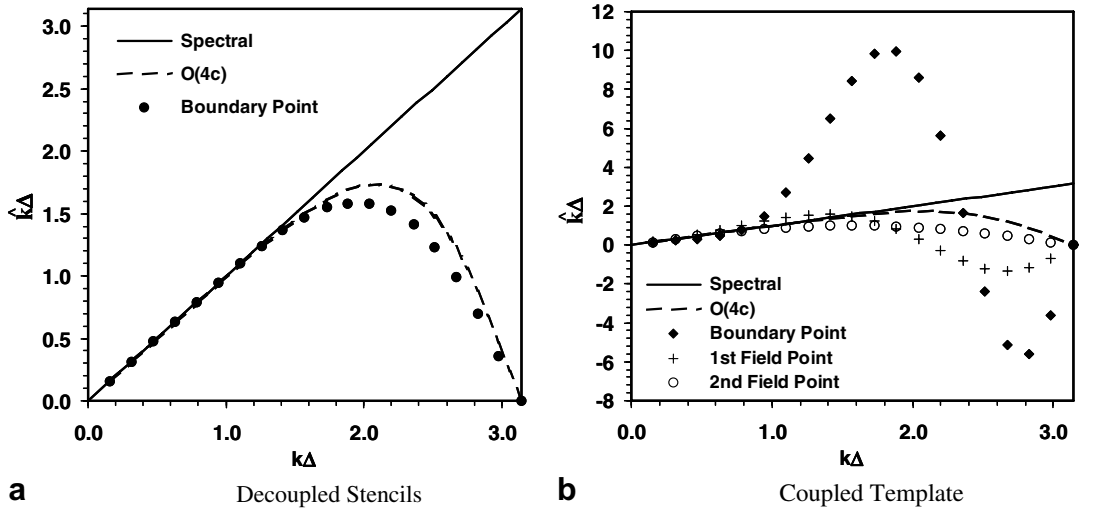

Fig. 4. Dispersive error distributions of Lele [7] composite compact finite difference template (2^2-4-2^2); 2^2: two-parameters ($a = 4$, $\lambda = -1/2$) second-order accurate on boundary, 4: fourth-order accurate in interior.

profile. Even the second interior point still indicates considerable dispersion over the upper 3/4s of resolvable scales $e(\delta_{90}) \leqslant 0.25$. This new understanding of the true spatial resolution is equally reflective of the dissipative error (not shown). This error only becomes negligible once past the second interior nodal point.

Other noteworthy samples of misleading resolution properties at the boundary (and adjacent interior points) include the composite templates derived by Cook and Riley [22] and Kim and Lee [13]. The former composite template comprised a sixth-order Pade-type interior scheme coupled with fifth-order compact stencils at the boundary and first interior points (template 5-5-6-5-5). The latter work derived a complex composite template that optimized two free parameters of separate spectral-like stencils at the boundary, first, second, and remaining interior points. The formal order of each stencil was second, fourth, sixth, and sixth, respectively (template 2^2-4^2-6^2-6^2-6^2-4^2-2^2). Only the dispersive errors of these composite templates are displayed in Fig. 5. One can quickly see that each boundary stencil approaches the dispersive errors similar to that of

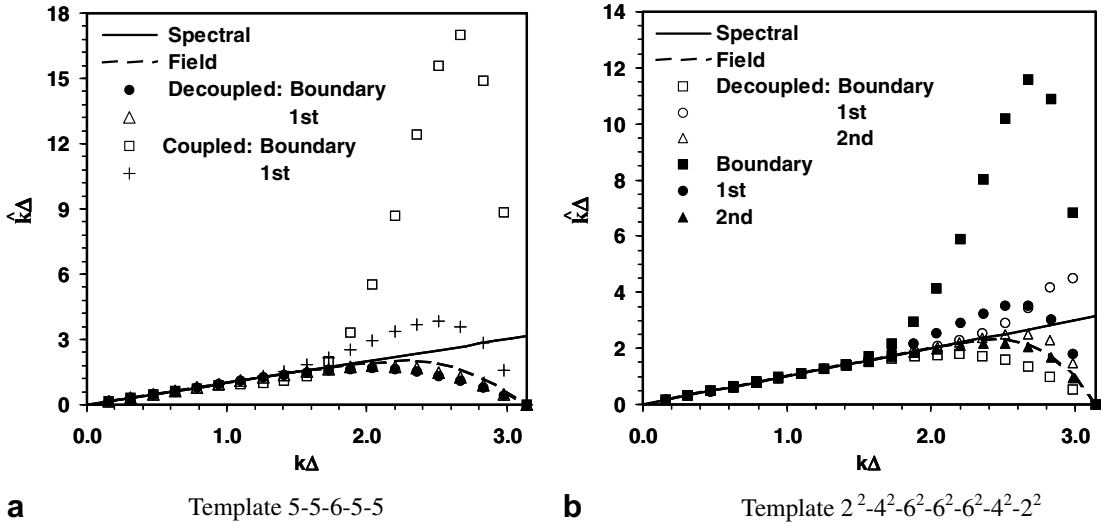

Fig. 5. Dispersive errors of composite finite difference templates (a) (5-5-6-5-5)[22] and (b) (2^2-4^2-6^2-6^2-6^2-4^2-2^2)[13]; solid symbols in (b) symbolize coupled determinations.

the field scheme when the modified wave number of the composite template is evaluated in a decoupled fashion. But like the previous examples, the dispersive errors are in fact quite large and broad banded at the boundary, which would actually demand fine gridding to minimize their local effect on the resolved scales of motion.

One final comment concerning the optimized composite template of Kim and Lee [13] is the sign change of the decoupled imaginary component at the boundary over the upper half of resolvable wavenumbers (see Fig. 6). They noted that this condition leads toward unstable solutions. But in their actual computations of linear and nonlinear wave propagation, Kim and Lee further noted no difficulties with maintaining stability. Realistically, this latter behavior should have been expected because the boundary dissipation of their composite template over the higher resolvable scales is actually quite large.

3.3. Optimizing template parameters

Attempting to reproduce the field resolution properties at the boundary is a difficult task because the governing system is over-determinate. The procedure requires a free parameter for every constraint used to reproduce the spectrum, but their availability clearly has practical limitations. The match is somewhat simplified for the compact central difference stencil because the imaginary component of the respective modified wavenumber is trivial. Thus, only one constraint (and free parameter) is needed to match the entire spectrum. But when aiming to mimic the corresponding dispersive error profile, small amounts of dissipative error are almost unavoidable.

One option for reproducing both field spectra concurrently is to apply a least-squares technique to the governing expressions such as those of (3.6) for the second-order-accurate two-parameter system (a, λ). Accordingly, their vector forms can be written as

$$q_i a = b_i + r_i \lambda \quad \text{and} \quad s_i a = d_i + t_i \lambda \tag{3.7}$$

where the subscript (i) denotes the number of wavenumber increments chosen to replicate the field spectrum. Rearranging these forms into unique expressions for each free parameter gives

$$S_i a = R_i \quad \text{and} \quad T_i \lambda = Q_i \tag{3.8a}$$

where

$$S_i = q_i t_i - r_i s_i, \quad R_i = b_i t_i - d_i r_i \quad \text{and} \quad T_i = r_i s_i - q_i t_i, \quad Q_i = s_i b_i - q_i d_i \tag{3.8b}$$

We now seek representative values for the free parameters (a, λ) by minimizing their error through a least-squares approach. By defining the square of the errors E and F as

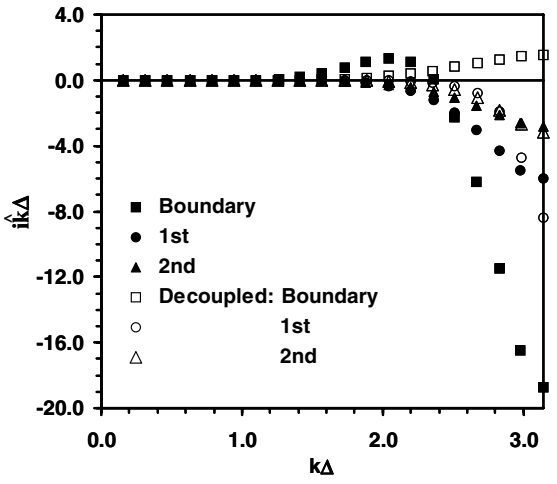

Fig. 6. Dissipative error of composite finite difference template $(2^2\text{-}4^2\text{-}6^2\text{-}6^2\text{-}6^2\text{-}4^2\text{-}2^2)^{13}$; solid symbols identify coupled determinations.

$$E = (R_i - S_i a)^2 \quad \text{and} \quad F = (T_i - Q_i \lambda)^2 \tag{3.9}$$

and setting $\partial E/\partial a = \partial F/\partial \lambda = 0$, the free parameters are evaluated as

$$a = (R_i S_i)/S_i^2 \quad \text{and} \quad \lambda = -(T_i Q_i)/T_i^2 \tag{3.10}$$

Note that the above expressions for the two-parameter family cannot become singular because their denominators can only approach zero if the numerator concurrently vanishes as well.

For the present illustrations of the least-squares approach, we will skip further treatment of the system in (3.6) because the second-order-accurate boundary stencil does not preserve fourth-order accuracy in the field. Instead, we will switch the boundary definition to a third-order-accurate two-parameter family (2.9). In their non-simplest form, the vector forms in (3.7) become

$$\begin{aligned}
q_i &= -6\hat{k}_\mathrm{r}^\mathrm{f} \sin k\Delta - 6\hat{k}_\mathrm{i}^\mathrm{f} \cos k\Delta + \cos 3k\Delta - 6\cos 2k\Delta + 3\cos k\Delta + 2 \\
s_i &= 6\hat{k}_\mathrm{r}^\mathrm{f} \cos k\Delta - 6\hat{k}_\mathrm{i}^\mathrm{f} \sin k\Delta + \sin 3k\Delta - 6\sin 2k\Delta + 3\sin k\Delta \\
b_i &= 6\hat{k}_\mathrm{i}^\mathrm{f} + 2\cos 3k\Delta - 9\cos 2k\Delta + 18\cos k\Delta - 11 \\
d_i &= -6\hat{k}_\mathrm{r}^\mathrm{f} + 2\sin 3k\Delta - 9\sin 2k\Delta + 18\sin k\Delta \\
r_i &= 6\cos 4k\Delta - 24\cos 3k\Delta + 36\cos 2k\Delta - 24\cos k\Delta + 6 \\
t_i &= 6\sin 4k\Delta - 24\sin 3k\Delta + 36\sin 2k\Delta - 24\sin k\Delta
\end{aligned} \tag{3.11}$$

where the free parameters of the finite difference stencil are (a,ξ). Applying the least-squares technique (3.10) over all resolvable wavenumbers $k\Delta \leqslant \pi$ (100 increments) evaluates the free parameters as $a = 3.5$ and $\xi = 0.10408$ to produce a suitable match between the boundary expression and a fourth-order Pade-type interior scheme. The remaining coefficients of the boundary stencil are evaluated using the relationships in (2.9).

Spectral distributions of the dispersive and dissipative errors at the boundary as determined for both the decoupled and coupled optimized composite template (3^2-4-6-4-3^2) are shown in Fig. 7. While the decoupled boundary spectra suggest profiles *well-matched* to the interior scheme, the actual distributions are quite poor. Apparently, emphasizing a least-squares minimization over all resolvable wavenumbers does not guarantee improvement of the resolution character of the two-parameter boundary stencil. A reasonable alternative may be to target the best partial match over a sub-set of resolvable scales ($k\Delta < \pi$). This idea proved appropriate for the boundary stencil as shown by the spectra in Fig. 8. By restricting the match to $k\Delta \leqslant \pi/2$, 56% of the resolvable waves now hold a 90% or better resolution efficiency; $e(\delta_{90}) \leqslant 0.56$. This improvement is nearly

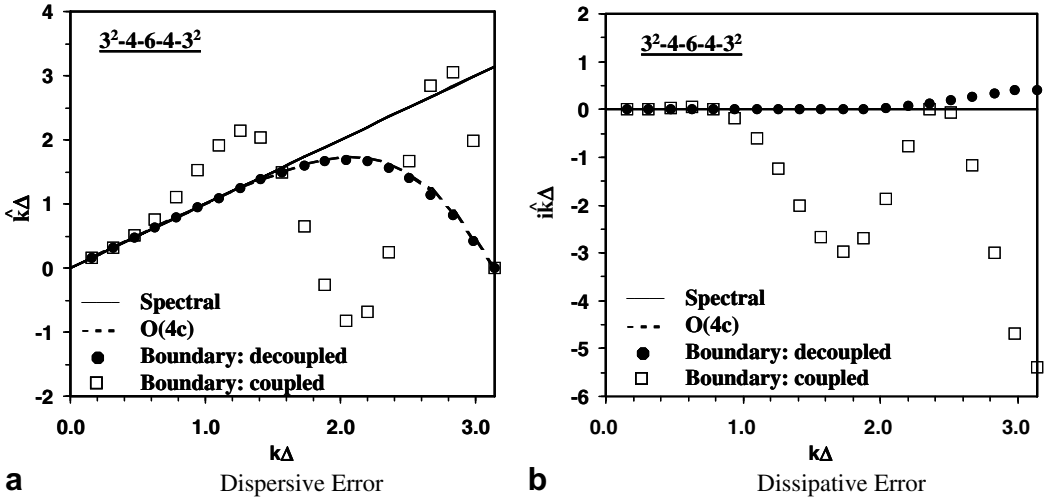

Fig. 7. Dispersive and dissipative error distributions of composite compact finite difference template (3^2-4-6-4-3^2); 3^2: least-squares optimization of two parameter family, third-order accurate on boundary, 4: fourth-order accurate at first adjacent point, 6: sixth-order accurate at field points.

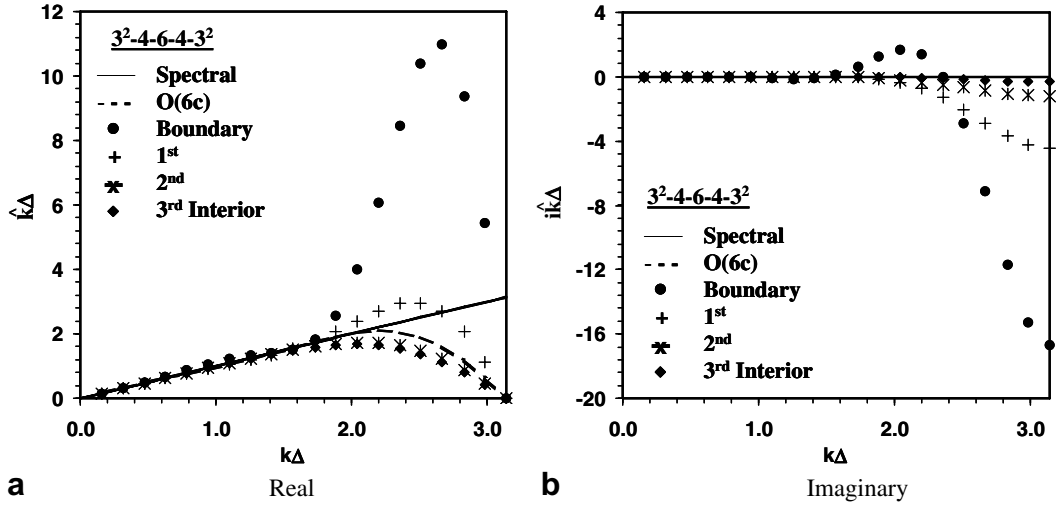

Fig. 8. Coupled dispersive and dissipative error distributions (partial least-squares fit, $k\Delta \leqslant \pi/2$) of optimized composite template (3^2-4-6-4-3^2); see notation in previous figure.

Table 3
List of coefficients for several one-sided two-parameter stencils with least-square minimization technique to the interior scheme; example notation (3^2-4-5-4-3^2), 3^2: two parameter family, third-order accurate on boundary, 4: fourth-order accurate at first adjacent point, 5: fifth-order-accurate upwinding in remaining interior

Template	a	η	δ	λ	α	γ	β
2^2-4-2^2	3.00000	–	–	−0.40429	2.21287	0.78713	−2.59571
3^2-4-3^2	3.50360	–	0.04198	−0.41852	2.25548	1.08028	−2.95922
4^2-4-4^2	3.64975	−0.00533	0.08080	−0.54485	2.52794	0.93189	−2.99044
3^2-4-5-4-3^2	3.50000	–	0.5299	−0.46195	2.31792	1.03805	−2.94701
4^2-4-5-4-4^2	3.58423	−0.01684	0.13287	−0.62715	2.54472	0.92896	−2.96255
3^2-4-6-4-3^2	3.50000	–	0.06025	−0.49099	2.36148	1.00901	−2.93975
4^2-4-6-4-4^2	3.58423	−0.01684	0.13287	−0.62715	2.54472	0.92896	−2.96255

double that of the standard one-sided third-order compact stencil $e(\delta_{90}) \leqslant 0.28$. Coincidentally, the first interior point holds better resolution properties than the remaining field.

One should note at this point that the least-squares procedure achieved lowest resolution errors at the boundary when the free parameters of the corresponding one-sided stencil were optimized against the adjacent interior stencil regardless of the number of separate participating schemes in the composite template. Although Table 3 lists different optimized values for the free parameters of each third-order two-parameter stencil at the boundary, the variations in modified wavenumber were only subtle. Essentially, determination of the parameters (a, ξ) in the third-order two-parameter family at the boundary were suitable for all composite templates tested herein that own a fourth-order Pade-type stencil at the adjacent interior point; i.e. templates 3^2-4-3^2, 3^2-4-6-4-3^2, etc.

4. Applications of the composite templates

Solving the one-dimensional linear convection and nonlinear Burgers equations should supply sufficient evidence for correlating the resolution properties of the present composite templates with their predictive error. More specifically, we seek to quantify the local effects of the dispersive and dissipative errors of the compact boundary stencil on the resolved wave amplitudes and phase for various uniform grid spacing. These computations involve placing a fictitious wall far downstream from the initial wave position where we can assess the predicted exit state of the single wave relative to the exact solution.

The governing system for one-dimensional propagation of a linear wave was previously presented in Eqs. (2.4) and (2.5). The corresponding nonlinear form of Burgers equation appears as

$$u_t + uu_x = \mu u_{xx} \tag{4.1}$$

where the convective derivative is non-conservative and partially stabilized by the pseudo-viscous parameter (μ). We choose the advective form of Burgers equation to facilitate treatment of both the central and upwind field templates. At initial time $t = 0$, the exact wave is

$$u(x, t = 0) = 1 - \tanh\left(\frac{x}{2\mu}\right) \tag{4.2a}$$

with the equivalent wave for all times defined by

$$u(x, t) = 1 - \tanh\left(\frac{x'}{2\mu}\right) \tag{4.2b}$$

where as before $x' = x - x_0 - t$. Inasmuch as we desire to isolate the resolving power of the present composite templates as applied to the convective derivative, the exact form of the pseudo-viscous term μu_{xx} was used in the computations;

$$\mu u_{xx} = \frac{1}{2\mu}\,\mathrm{sech}^2(v')\tanh(v') \tag{4.3}$$

where $v' = x'/2\mu$. With the viscous term present, each wave was time advanced using the second-order-accurate Adams–Bashforth scheme. But like the linear convection computations, a small CFL value was chosen to minimize the truncation error of the time derivative approximation.

Two solutions that highlight application of a standard and optimized composite template (notations 3-4-6-4-3 and 3^2-4-6-4-3^2) to the advective term in Burgers equation are shown in Figs. 9a,b, 10a and b. Both compact templates are asymptotically stable and theoretically preserve their formal order at the interior nodal points. The corresponding modified wavenumber spectra were discussed previously (Figs. 3 and 8) where the latter template reflects an optimized two-parameter family boundary stencil by the least-squares technique (3.10). Four uniform grids were tested that varied from very coarse to fine spatial resolution; $k\Delta \sim 3\pi/4$, $\pi/2$, $\pi/4$ and $\pi/16$. The fictitious wall was placed 100 time units downstream of the initial wave position.

All four figures reveal improved predictions of the peak wave amplitude ($x' = 0$) with reduced grid spacing. Not surprisingly, the coarsest grid results ($k\Delta \sim 3\pi/4$) indicate a degradation of the wave amplitude and phase by the optimized composite template (3^2-4-6-4-3^2). This result correlates well with its much larger dispersive error. Apart from the coarsest spacing, this template gives a superior gain in the predictive accuracy as echoed by its better overall resolution quality at the midrange to lower resolvable scales. For the finest grid ($k\Delta \sim \pi/16$),

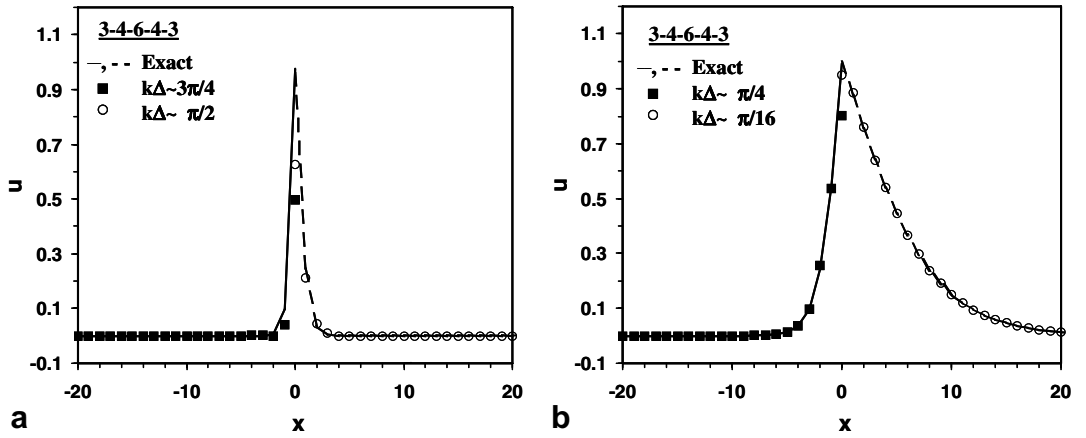

Fig. 9. Solutions of Burgers equation using composite template 3-4-6-4-3.

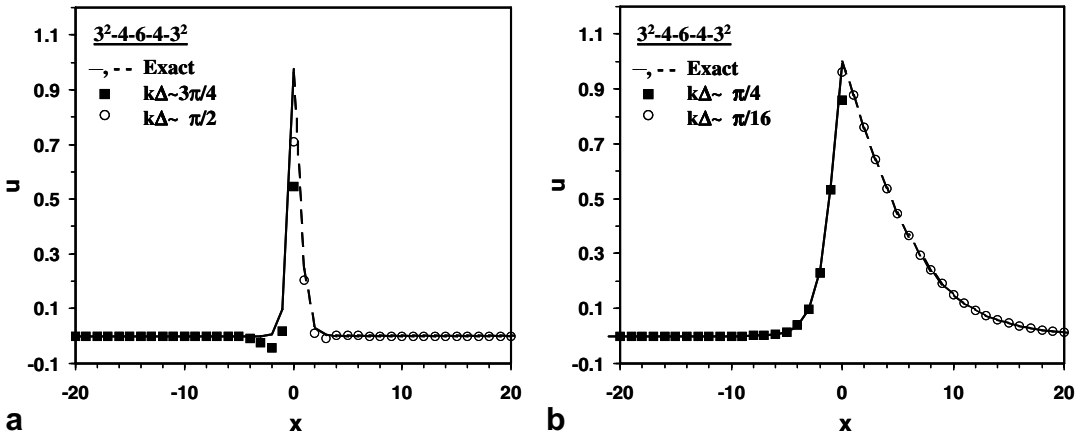

Fig. 10. Solutions of Burgers equation using composite template 3^2-4-6-4-3^2.

the results of both templates are almost indistinguishable. But this comparison is again not unexpected because the resolution efficiency of the optimized compact template is only slightly improved over its counterpart 3-4-6-4-3 template at the fine spacing $k\Delta \sim \pi/16$; $\delta_r = 98\%$ (3-4-6-4-3) versus $\delta_r = 99\%$ (3^2-4-6-4-3^2).

Outside of the 2-4-2 composite, the above discussion and accompanying figures are qualitatively typical of the remaining compact templates tested herein for advancing Burgers wave to the fictitious wall boundary. We can obtain a clearer picture of each by evaluating their ability to predict the exact wave. The predictive errors as quantified by the L_2 norm of eight composite templates are plotted in Fig. 11 where $\|L_2\| = [\sum |u_e - u_{fd}|^2]^{1/2}$. Each compact template was tested over the same four grid spacings ($k\Delta \sim 3\pi/4$, $\pi/2$, $\pi/4$ and $\pi/16$) with the respective errors calculated using one-half of the wave once centered over the fictitious wall (100 time units). The predictive errors of the stencil mixtures (3-4-6-4-3), $(2^2\text{-}4\text{-}2^2)^7$, $(5\text{-}5\text{-}6\text{-}5\text{-}5)^{22}$ and $(2^2\text{-}4^2\text{-}6^2\text{-}6^2\text{-}6^2\text{-}4^2\text{-}2^2)^{13}$ are those previously discussed and correlate with the wave number spectra in Figs. 3–5. Also, evaluation of the L_2 norm from solutions of the 4c scheme with periodic boundary conditions is included to demonstrate proper convergence of Burgers equation with finer grid spacing.

Interestingly, no compact template converged on their formal order at the boundary. Outside of the two-parameter family scheme $(2^2\text{-}4\text{-}2^2)^7$, the templates share similar reductions of predictive error. All eight templates as tested under the finest grid ($k\Delta \sim \pi/16$) show the lowest errors, which by comparison are barely separable. This observation agrees well with their equally low dispersive and dissipative errors. In Fig. 11, the

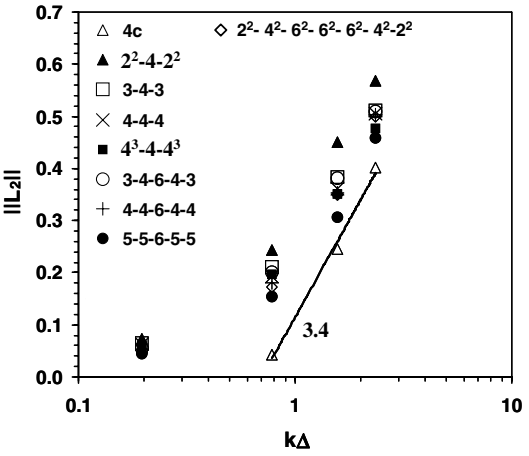

Fig. 11. Predictive errors (L_2 norm) of eight composite templates as applied to Burgers equation; $\|L_2\| = [\sum |u_e - u_{fd}|^2]^{1/2}$.

most discernible disparity among the predictive errors occurs at the intermediate grid densities. And these differences also correlate with their respective spatial resolution errors as well as their formal accuracy at the boundary. For example, lowering the stencil accuracy at the wall boundary, such as sequentially from (5-5-6-5-5)[22] to (4-4-6-4-4) to (3-4-6-4-3), degraded their resolution power and concurrently raised the predictive error. We note that this trend of performance specifically at the boundary agrees with previous observations [3,20] regarding the field accuracy.

An attempt to reduce the predictive error of seven traditional composite templates (no free parameters) by switching the boundary stencil to a two-parameter family is shown in Fig. 12. These templates included compact central (4c and 6c) as well as compact upwind (5c) schemes at the field nodal points. Each boundary stencil was optimized by the least-squares procedure (3.10) where the respective values for the free parameters are listed in Table 3. Generally, optimizing both boundary parameters over 50–70% of the lower resolvable wavenumbers generated the best overall improvement in predictive accuracy at all grid densities. At first glance, the larger optimized stencils lowered the predictive error regardless of the formal order either at the boundary or in the field with only minor improvements seen using the finest grid. Comparisons to their respective resolution spectra show good agreement with this trend. Essentially, the resolution errors varied considerably at the coarsest spacing ($k\Delta \sim 3\pi/4$) whereas they are consistently similar at the lowest resolvable scales. In view of all the optimized templates, the 2^2-4-2^2 mixture clearly displays the largest gain in predictive accuracy over its companion traditional scheme.

Quantifying the improvement as a percent reduction of predictive error is illustrated in Fig. 13 for six compact templates where the most substantial gains of each template are visibly evident at the intermediate grid densities. Among the six templates, the peak improvements come from those owning the leading differences between the formal orders of the boundary and field schemes. Ostensibly, the optimized boundary stencil compensates for a lost in predictive accuracy when it is lower than one order ($>p\text{th} - 1$) from the final interior scheme. However, this result surfaces only when the free parameters are optimized against the compact scheme at the first adjacent point. These final observations lead us to conclude that the larger optimized stencils at the boundary can diminish the predictive error of the compact template regardless of the remaining composition in the interior field.

Predictions of the linear wave propagation to the exit boundary (400 time units) by the six optimized composite templates are shown in Fig. 14a. Unlike the applications to Burgers equation, the higher-order field templates gave lowest errors. But as expected, this difference diminished under the finest grid spacing ($k\Delta \sim \pi/16$) because their dispersive errors at this spatial resolution are essentially equivalent. As observed previously in the Burger wave predictions, none of the boundary stencils converged on their formal order with

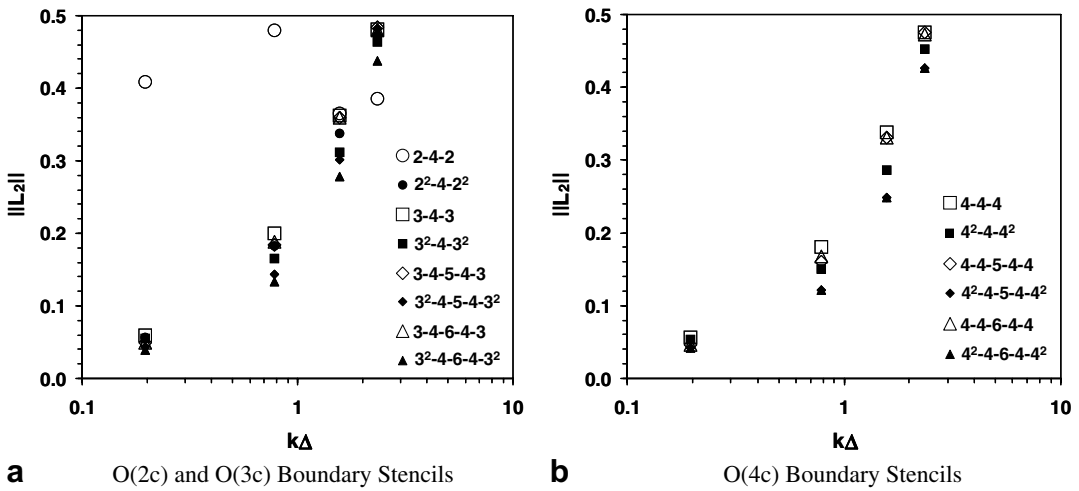

Fig. 12. Predictive errors (L_2 norm) of composite templates including optimized multi-parameter family stencils at the boundary as applied to Burgers equation.

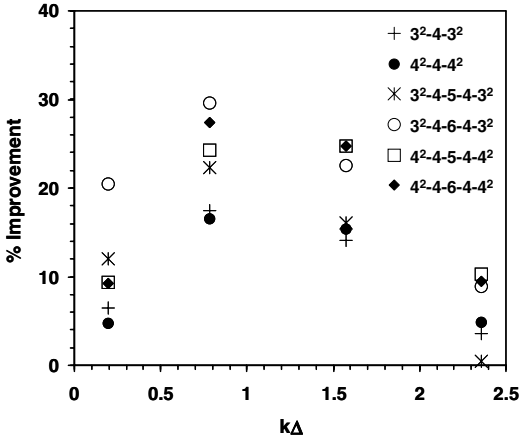

Fig. 13. Percent improvement of predictive error after switching boundary stencil from the standard to an optimized multi-parameter family expression.

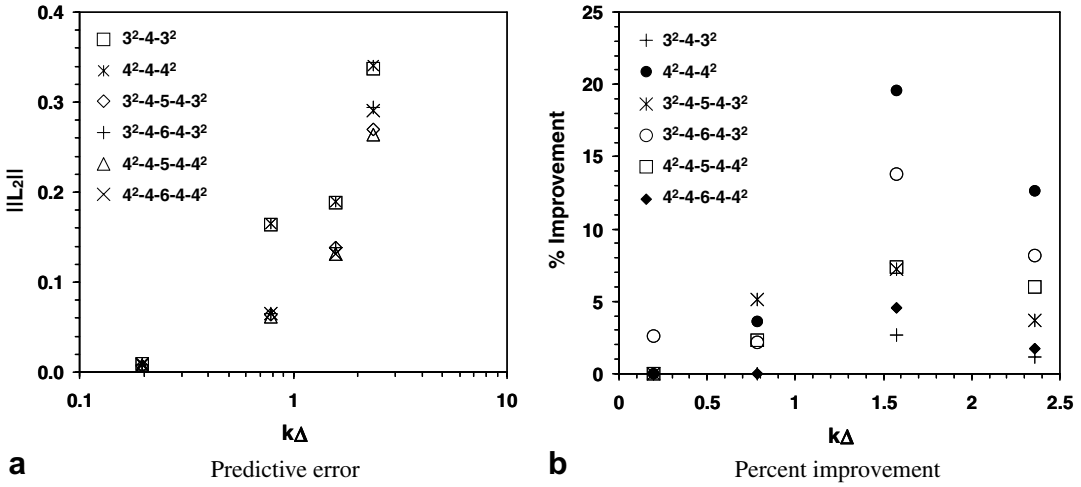

Fig. 14. Predictive errors (L_2 norm) and percent improvement of optimized composite templates as applied to the linear convection equation.

reduced grid spacing. Typically, the larger templates gave no better than second-order convergence. Improvement in the predictive error of the pure wave at exit between the respective standard and optimized templates is illustrated in Fig. 14b. Recomputing the linear wave using the optimized templates follows a trend similar to the Burgers wave predictions, but their levels of error improvement are noticeably lower.

5. Final remarks

Every composition of two or more compact finite differencing stencils own three global characteristics that are clearly fundamental to our expected understanding. These properties center on the composite's stability, accuracy and resolution. Prior to the present effort, only the field accuracy and global stability were properly analyzed as a fully coupled system. The spatial resolution in terms of their dispersive and dissipative errors was routinely quantified as unique properties of each participating stencil that were independent from their neighboring schemes. Herein, observations of the local resolution errors between the decoupled and coupled templates clearly reveal that each stencil is strongly linked within the composite. While a close separate match can appear between a multi-parameter family stencil at the boundary and the adjacent interior scheme, their

coupled profiles prove otherwise. Typically, the dispersive and dissipative errors of the boundary stencil over the upper half of resolvable scales bear little resemblance to the corresponding resolution efficiency within the field. Herein, we moderately relax this discrepancy by developing a least-squares method to optimize the multi-parameter family stencils. Solutions of the linear convection and Burgers equations showed best improvements in the template accuracy over the intermediate range of resolvable scales.

Notably, many solution errors arise when applying composite compact finite differencing to resolve the fine scale physics. The present work only isolates those errors resulting from their reduced resolving properties as compared to a perfect resolution approach like spectral methods. Other effects such as intermittent explicit filtering complicate the analysis. Jordan [23] showed that explicit filtering modifies the resolvable wavenumbers twice leading to higher resolution errors as given by the respective wavenumber spectra. Thus, the procedure develop here to quantify the resolution properties of composite compact templates requires further adjustments to account for the coupling effects of explicit filtering.

We reemphasize that the multi-parameter family stencils were optimized against the adjacent (not final) interior scheme to yield the best performance with lower resolution errors of the respective composite template. For instance, the free parameters of the 3^2-4-6-4-3^2 template were optimized using the spectra of the adjacent 4c stencil rather than the final 6c scheme. One apparent improvement to this approach may be to first optimize the free parameters of an extended 4c stencil to the 6c scheme, then complete the template by subsequently optimizing the boundary scheme. This approach should lead to an improved resolution character of the composite compact template over a wider range of resolvable wavenumbers.

Lastly, projecting this new understanding to three-dimensional applications such as resolving turbulence and acoustic characteristics sparks many issues. Apparently, raising the formal order of the field template does little to raise the near wall resolution. One should only expect negligible improvement in the local predictions by simply substituting a higher-resolution compact interior scheme along grid lines tangential to the boundary. Focus must be centered on lowering the resolution errors of the local compact stencils themselves. This reduction is possible by replacing the standard compact one-sided scheme and adjacent stencils with optimized free-parameter families by a least-squares technique (or similar method). The superior spatial resolution will propagate far into the interior while concurrently easing the demand for local fine grid spacing. This argument equally applies to the field solutions where grid discontinuities such as branch cuts and sub-domain boundaries call for stencils dissimilar from the field. Global analyses of the composite field template should take place prior to the computation to properly understand their prevailing resolution properties as well as their stability and accuracy.

Acknowledgments

The author gratefully acknowledges the support of the Office of Naval Research (Dr. Ronald D. Joslin, Program Officers), Contract No. N0001406AF00002. The computational work was supported in part by a grant of HPCMP resources from the Arctic Region Supercomputing Center (ARSC) and the Naval Oceanographic Office Major Shared Resource Center (NAVO MRSC).

References

[1] R.S. Hirsh, Higher order accurate difference solutions of fluid mechanics problems by a compact differencing technique, Journal of Computational Physics 19 (1975) 90–109.
[2] Y. Adam, Highly accurate compact implicit methods and boundary conditions, Journal of Computational Physics 24 (1977) 10–22.
[3] B. Gustafsson, Highly accurate compact implicit methods and boundary conditions, Mathematics of Computation 29 (130) (1975) 396–406.
[4] I. Christie, Upwind compact finite difference schemes, Journal of Computational Physics 59 (3) (1985) 353–368.
[5] N.N. Mansour, P. Moin, W.C. Reynolds, J.H. Ferziger, Improved methods for large-eddy simulation of turbulence, in: Turbulent Shear Flows I, Springer, Berlin, 1979, pp. 386–400.
[6] N.D. Sandham, W.C. Reynolds, Three-dimensional simulations of large eddies in the compressible mixing layer, Journal of Fluid Mechanics 224 (1991) 133–158.
[7] S.K. Lele, Compact finite difference schemes with spectral-like resolution, Journal of Computational Physics 103 (1992) 16–42.
[8] R.D. Joslin, Direct simulation of evolution and control of three-dimensional instabilities in attachment-line boundary layers, Journal of Fluid Mechanics 291 (1995) 369–392.

[9] N.A. Adams, K. Shariff, A high-resolution hybrid compact-ENO scheme for shock-turbulence interaction problems, Journal of Computational Physics 127 (1996) 27–51.
[10] R. Hixon, E. Turkel, High-accuracy compact MacCormack-type schemes for computational acoustics, in: 36th AIAA Aerospace Sciences Meeting, AIAA paper 98-0385, 1998.
[11] C. Hardin, J.R. Ristorcelli, C.K.W. Tam, in: ICASE/LaRC Workshop on Benchmark Problems in Computational Aeroacoustics, NASA CP-3300, Hampton, VA, 1995.
[12] C.K.W. Tam, C. Hardin, in: Second Computational Aeroacoustics (CAA) Workshop on Benchmark Problems, NASA CP-3352, Hampton, VA, 1997.
[13] J.W. Kim, D.J. Lee, Implementation of boundary conditions for optimized high-order compact schemes, Journal of Computational Acoustics 5 (2) (1997) 177–191.
[14] M. Popescu, W. Shyy, M. Garbey, Finite-volume treatment of Dispersion-Relation-Preserving and Optimized-Prefactored-Compact schemes for wave propagation, Report UH-CS-05-03, Department of Computer Science, University of Houston, Houston, TX, 2005.
[15] C.K.W. Tam, J.C. Webb, Dispersion-Relation-Preserving schemes for computational acoustics, Journal of Computational Physics 103 (1993) 262–281.
[16] G. Ashcroft, X. Zhang, Optimized prefactored compact scheme, Journal of Computational Physics 190 (2003) 459–477.
[17] C. Rosales, Modeling of turbulent premixed combustion, in: Johns Hopkins ME Seminar, 2003.
[18] S.C. Li, Cavitation of Hydraulic Machinery, World Scientific Publishing Company, Singapore, 2001.
[19] E. Turkel, High order methods, in: A. Taflove (Ed.), Advances in Computational Electrodynamics: The Finite-Difference Time-Domain Method, Artech House, Boston, 1998, pp. 63–109.
[20] M.H. Carpenter, D. Gottlieb, S. Abarbanel, The stability of numerical boundary treatments for compact high-order finite-difference schemes, Journal of Computational Physics 108 (1993) 272–295.
[21] Y.M. Chung, K.H. Luo, Unsteady heat transfer analysis of an impinging jet, Journal of Heat Transfer 124 (2002) 1039–1047.
[22] A.W. Cook, J.J. Riley, Direct numerical simulation of a turbulent reactive plume on a parallel computer, Journal of Computational Physics 129 (2) (1996) 263–283.
[23] S.A. Jordan, Resolving turbulent wakes, Journal of Fluids Engineering 125 (2003) 823–834.